2020-01-02

Individual violent wave-overtopping events: behaviour and estimation

Raby, Alison

10.1080/00221686.2018.1555549
Journal of Hydraulic Research
Taylor & Francis

Journal of Hydraulic Research

ISSN: 0022-1686 (Print) 1814-2079 (Online) Journal homepage: https://iahr.tandfonline.com/loi/tjhr20

Individual violent wave-overtopping events: behaviour and estimation

Alison Raby, Ravindra Jayaratne, Henrik Bredmose & Geoff Bullock

To cite this article: Alison Raby, Ravindra Jayaratne, Henrik Bredmose & Geoff Bullock (2019): Individual violent wave-overtopping events: behaviour and estimation, Journal of Hydraulic Research, DOI: 10.1080/00221686.2018.1555549

To link to this article: https://doi.org/10.1080/00221686.2018.1555549

Journal of Hydraulic Research, 2019
https://doi.org/10.1080/00221686.2018.1555549

Research paper

Individual violent wave-overtopping events: behaviour and estimation

ALISON RABY, Professor, *School of Engineering, University of Plymouth, Plymouth, UK*
Email: alison.raby@plymouth.ac.uk (author for correspondence)

RAVINDRA JAYARATNE, Senior Lecturer, *School of Architecture, Computing and Engineering, University of East London, Docklands Campus, 4-6 University Way, London, UK*
Email: r.jayaratne@uel.ac.uk

HENRIK BREDMOSE, Professor, *DTU Wind Energy, Nils Koppels Allé Building 403, Kongens Lyngby DK-2800, Denmark*
Email: hbre@dtu.dk

GEOFF BULLOCK, Emeritus Professor, *School of Engineering, Plymouth University, Plymouth, UK*
Email: gbullock@plymouth.ac.uk

ABSTRACT
To better understand individual violent wave overtopping, of significance for coastal defence design, three breaking wave types (steep-fronted, plunging and broken) based on focused wave groups, were generated in laboratory and numerical models. High-speed video captured overtopping events and produced velocity vector maps by means of bubble image velocimetry (BIV). Results were compared with a numerical model based on a linear wave detection procedure and a two-phase incompressible Navier–Stokes-based solver. This novel approach revealed that the overtopping waves comprised an initial jet of 0.2 s duration, but dominated by quasi-steady flow. Whilst laboratory surface-elevation time-histories were highly repeatable, overtopping volume repeats were sensitive to the breaker type. Measured volumes were compared with: the numerical model (which over-predicted, but was reasonably accurate for steep-fronted waves); estimations based on BIV results (which provided very close agreement for the steep-fronted waves); and a weir-based analogy (which provided reasonable agreement, but always under-predicted).

Keywords: Breaking waves; bubble image velocimetry; coastal engineering; flow visualization and imaging; incompressible Navier–Stokes solver; laboratory studies; violent wave overtopping

1 Introduction

The assessment of overtopping rates is often one of the most important considerations when designing a new seawall or breakwater. Because the individual overtopping volumes are highly variable, the assessment is often limited to the prediction of the mean overtopping discharges for various sea states and most investigations into wave overtopping have been directed towards this end. Whilst this may be satisfactory for some purposes, it is an individual overtopping event that sweeps unwary pedestrians off their feet or causes car drivers to take evasive action. EurOtop (2016) highlights the fact that it is difficult to visualize individual wave overtopping volumes from average discharges. Furthermore, Nørgaard, Andersen, Burcharth, and Steendam (2013) comment that dike designs are typically based on mean overtopping discharge and that this is inappropriate for coupling the failure with individual overtopping volumes. Thus, in some situations, the ability to both predict and characterize large overtopping events can be of crucial importance. Methods for estimating maximum overtopping events are currently based upon an assumed probability distribution of volumes (e.g. Burcharth & Hughes, 2006; EurOtop, 2016). There are other approaches that use a deterministic, physics-based approach but these are limited to gentle slopes up to a steepness of 1:3 (Hughes & Nadal, 2009; Hughes & Thornton, 2016).

As a contribution towards an improved understanding of individual violent wave overtopping behaviour, the present paper provides physical and numerical modelling observations arising from the violent impact on a sloping wall of three distinct types of breaker, namely steep-fronted, plunging and already-broken. The wall had a plane slope at 27° to the vertical and three different crest elevations. In the laboratory, overtopping

Received 13 April 2017; accepted 30 November 2018/Currently open for discussion.

ISSN 0022-1686 print/ISSN 1814-2079 online
http://www.tandfonline.com

flow depths were obtained from the video images and overtopping volumes using a catchment box. Bubble image velocimetry (BIV) was used to indicate the velocity field in the aerated regions. A numerical technique based upon a Navier–Stokes solver reproduced the experiments. Differences in behaviour of the three breaker types are discussed, and overtopping estimates based on three different methods are compared with physical measurements.

The paper is organized in sections as follows: Section 2, literature review; Section 3, experimental set-up; Section 4, details of the numerical model; Section 5, overtopping results from both the physical and numerical models, including observations and comparisons of the overtopping estimation techniques; Section 6, discussion and conclusions.

2 Literature

Over the past 20 years, considerable progress has been made with the prediction of mean overtopping rates. This has included advances in design predictions for random seas; field tests to investigate issues of scale; consideration of breaking wave conditions; predictions using neural networks based on databases; and estimations of tolerable discharges. Substantial European projects such as OPTICREST (The Optimization of the Crest Level Design of Sloping Coastal Structures through Prototype Monitoring and Modelling, De Rouck & Van de Walle, 2001), VOWS (Violent Overtopping by Waves at Seawalls, Pearson, Bruce, & Allsop, 2002) and CLASH (Crest Level Assessment of Coastal Structures by Full-scale Monitoring, Neural Network Prediction and Hazard Analysis Permissible Wave Overtopping, De Rouck, Verhaeghe, & Geeraerts, 2009) have built upon the seminal investigations of Van der Meer and Janssen (1995) and Besley (1999). Key findings are now incorporated in design guidance of the Coastal Engineering Manual (Burcharth & Hughes, 2006) and the recently revised EurOtop Manual (EurOtop, 2016). However, there is still little guidance that enables particular incident waves to be linked to individual overtopping events.

Empirical methods for predicting the overtopping over a $\beta°$ slope take some account of breaker type by incorporating the Iribarren number $\xi_{m-1,0} = \tan\beta/(H_{m0}/L_{m-1,0})^{1/2}$ into the procedure, where H_{m0} is the significant wave height at the toe of the structure, and $L_{m-1,0}$ is the deep water wavelength (EurOtop, 2016). However, $\xi_{m-1,0}$ is not a precise determinant of wave breaking and whether a wave is non-breaking, breaking or already broken can cause the overtopping to range from a gentle flow to water being projected high into the sky (Watanabe & Ingram, 2016). Besley (1999) noted differences in overtopping for breaking and reflecting waves on vertical structures, identifying the need for distinguishing between impulsive and non-impulsive conditions in design guidance (Bruce, van der Meer, Pullen, & Allsop, 2010).

Van der Meer and Janssen (1995) provided a method for estimating "maximum" overtopping volumes based upon a Weibull distribution for the exceedance of individual overtopping events. Such estimates were suggested as being more useful for safety purposes than mean values (Besley, 1999). Schüttrumpf and Oumeraci (2005) undertook an experimental and theoretical investigation into wave run-up and overtopping on parts of a sea-dike and found that the depth of the overtopping flow exhibited a rapid increase followed by a slower decrease. This flow characteristic was also detected by Hunt-Raby, Borthwick, Stansby, and Taylor (2011) who produced correlations of individual overtopping volumes with waves of different types for a modest-sloped plane wall. Using an engineering hydraulics approach, Dean, Rosati, Walton, and Edge (2010) determined individual overtopping volumes for grass covered levees by linking time-varying depth characteristics and steady-flow levee overtopping erosion relationships. Hughes and Nadal (2009) presented results from model levees that include distributions of overtopping discharge, individual volumes, and flow depths, of interest in this paper. More recently Hughes and Thornton (2016) scrutinized 5799 individual overtopping events to derive a two-parameter Weibull probability density function for wave discharge that they used to assess the resiliency of sea dike protection.

The aerated flows associated with breaking-wave overtopping can be investigated in a laboratory by means of BIV (Ryu, Chang, & Lim, 2005), which uses the principles of particle image velocimetry without the need for a laser because bubbles are used as tracers rather than being a source of errors. The technique works by comparing the textural change between consecutive video images. BIV experiments include: run-up and green water velocities due to breaking wave impinging and overtopping (Ryu, Chang, & Mercier, 2007); the estimation of velocity components in a turbulent bore in small-scale wave–structure interaction experiments (Antoine, 2009) and plunging breakers in the surf zone (Rivillas-Ospina, Pedrozo-Acuna, Silva, Torres-Freyermuth, & Gutierrez, 2012).

Numerical modelling techniques can now also be used to simulate the complex wave–structure interactions seen in overtopping events. Stansby et al. (2008) present results of solitary wave overtopping using several numerical methods: a Boussinesq model; a volume of fluid model, and SPH (smoothed particle hydrodynamics). They compared the model results with data from the UKCRF on a 1:2.17 structure (Hunt-Raby et al., 2011) and generally found close agreement, though the SPH model was the most effective for steeper structures. Orszaghova, Borthwick, and Taylor (2012) present comparisons of numerical predictions of wave overtopping using a Boussinesq shallow water numerical wave tank, based on Madsen and Sørensen's (1992) equations with data from the tests by Hunt-Raby et al. (2011); very close agreement was achieved. Latterly McCabe, Stansby, and Apsley (2013) have used a shallow water and Boussinesq (SWAB) model to predict random wave overtopping rates and maximum volumes, comparing them to experimental

data. The model generally over-predicted the overtopping levels by up to a factor of 2; however, it was also discovered that the measured cumulative overtopping varied by 25%, highlighting the sensitivity of overtopping to wave conditions.

3 Experimental set-up

3.1 *The test structure*

Physical modelling work was conducted in a 20 m long, 0.9 m wide, 1.2 m deep wave channel where the still water depth was set to 0.75 m. The channel was equipped with a computer-controlled wedge-type wave generator (Bullock & Murton, 1989) as illustrated schematically in Fig. 1.

A steep wall representative of a smooth impermeable seawall or breakwater was mounted opposite the generator. The wall was of modular design with its face built up from rectangular slabs of 25 mm thick polymer so that its crest could be set at 150, 200 or 250 mm above still water level (SWL). To minimize any flexing under wave impacts, the polymer slabs were bolted onto a steel frame that was securely attached to the bottom of the channel and sloped back at 27° to the vertical.

The wall was fronted by a 220 mm horizontal berm 150 mm below SWL and a 1:3 plane slope, as illustrated schematically in Fig. 1. This arrangement was designed with the aid of a numerical model based on the boundary integral solver of Dold and Peregrine (1986) to obtain steep and overturning impacts at the wall. Further details of the modelling set-up can be found in Bredmose, Hunt-Raby, Jayaratne, and Bullock (2010).

3.2 *Wave generation*

So that the individual overtopping events caused by a steep-fronted, a plunging and a broken wave could be investigated under repeatable and relatively undisturbed conditions, all tests were conducted using focused wave groups (e.g. Baldock, Swan, & Taylor, 1996; Hunt-Raby et al., 2011; Whittaker et al., 2017) and the water in the wave channel was allowed to settle for 15–20 minutes between tests. The group spectra and focus locations were manipulated so that: (a) the second wave in each group shoaled to form one of the required types of breaker at the wall, and (b) the impact of the breaker against the wall was sufficiently violent to cause significant overtopping for all the crest elevations used in the tests. The parameters used are listed in Table 1. A top-hat spectrum was used to produce the broken wave because the second wave in the group did not cause sufficient overtopping when a JONSWAP spectrum was used. A similar methodology was used by Kway, Loh, and Chan (1998), where different spectra were used to produce different types of deep-water breaker. The surface elevation time-histories were based upon the following equation:

$$\eta(x,t) = \alpha/\sigma^2 \sum_n S_\eta(\omega_n)\,\Delta\omega \cos\left(\omega_n (t - t_0) - k_n (x - x_0)\right) \tag{1}$$

where (x,x_0) is distance and focus point, (t,t_0) is time and focus time, n the counter for the sum, S_η the wave spectrum, σ the standard deviation of the free surface elevation, α the crest height, k_n the wave number, ω_n the frequency and $\Delta\omega$ the frequency discretization.

Wave data were sampled at 100 Hz by six wave gauges placed along the centre of the channel as shown in Fig. 1. Figure 2 shows 10 repeat tests of the surface elevation time histories measured by Gauge 3 (at the toe of the slope) for each of the three wave groups. The time axis was adjusted so that the crest of the second wave passed the toe of the structure (WG3) at $t = 0$ s. Figure 2 indicates that, at this location, the repeatability of the waves of interest was excellent as there

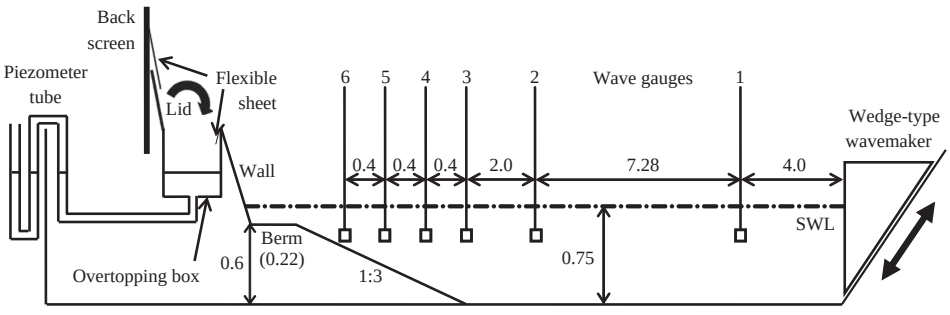

Figure 1 Schematic diagram of the structure with locations of wave gauges 1 to 6. All dimensions are in m

Table 1 Wave parameters

Breaking wave type	Underlying spectral shape	Spectral minimum, maximum and peak (Hz)	Focus location with respect to paddle (m)	Maximum wave height at toe of 1:3 slope (mm)
Steep-fronted	JONSWAP	0.293, 1.454 and 0.504	16.0	162
Plunging	JONSWAP	0.293, 1.454 and 0.504	13.3	205
Broken	Top-hat	0.293, 1.454 and N/A	8.0	233

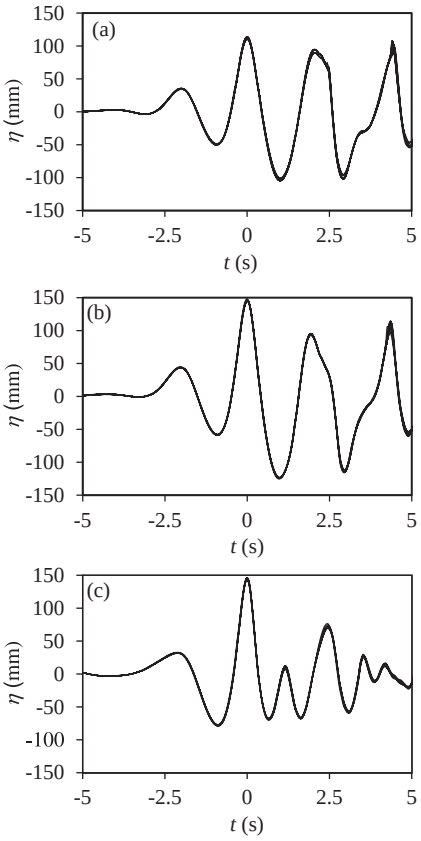

Figure 2 Ten repeat surface elevation time histories measured at the toe of the structure, 13.28 m from the paddle: (a) focused group producing a steep-fronted wave; (b) focused group producing a plunging wave; and (c) focused group producing a broken wave

are no discernible differences between the repeats until after the records are affected by reflections. The fact that the records become less repeatable once they contain a reflected component suggests that the reflection from impacting waves is somewhat variable and that the overtopping will also be variable to some degree.

The two groups that produced steep-fronted and plunging breakers look very similar but led to quite different interactions and overtopping volumes. The wave heights given in Table 1 are the preceding trough to crest values for the waves with crests at $t = 0$ s at WG3. Inspection of Fig. 2 indicates that the waves are far from fully characterized by this single parameter, which is included to illustrate the danger of making generalizations about overtopping based on simple wave parameters.

3.3 *Measurement of overtopping volumes*

The overtopping caused by the breaker of interest was measured over a 241 mm length of wall in the centre of the channel. Quantities were determined volumetrically using a rectangular collection box with internal dimensions of 225 × 219 × 250 mm ($L \times W \times D$) behind the wall as indicated in Fig. 1. The volume was determined by measuring the depth of water inside the box using a piezometer tube and point gauge, to a precision of ± 0.1 mm.

For some circumstances the wave following the one of interest also overtopped the structure. In these situations, a lid was quickly drawn over the collection box to prevent the capture of additional water.

3.4 *Bubble image velocimetry (BIV)*

BIV was used to reveal the flow characteristics within the breaking waves in areas where there was a good concentration of naturally entrained air bubbles. The bubbles were backlit to increase contrast, thereby improving the accuracy of the resulting velocity vector maps. The BIV velocity data are subsequently used to estimate overtopping discharge and hence overtopping volumes. Details of the BIV measurement system can be found in Jayaratne, Hunt-Raby, Bullock, and Bredmose (2008) and details of the validation method are provided in Supplemental Material S1.

4 Numerical modelling

Numerical reproduction of the experiments was made with a two-phase incompressible Navier–Stokes solver for the water and surrounding air in a simple 2D set-up. The solver was chosen due to its ability to model the full set-up of wave flume and overtopping region in a single numerical domain and due to previous good results in reproduction of experimental wave–structure interaction (Paulsen, Bredmose, & Bingham, 2014). The solver is based on the interFoam solver of the OpenFOAM® toolbox, version 2.1.x coupled with the "waves2Foam" toolbox (Jacobsen, Fuhrman, & Fredsøe, 2011). A good description of interFoam and MULES is provided by Deshpande, Anumolu, and Trujillo (2012).

The numerical grid for the present computations consists of 46,000 cells. At the wave-maker a horizontal grid spacing of 100 mm was applied while the cell size at the inclined wall was 7.5 mm × 7.5 mm. The numerical grid in the berm region is shown in Fig. 3.

The numerical model set-up is associated with a number of approximations. While the approximation of two-dimensional flow is considered accurate for the wave propagation until the berm top, transverse modulations of the impacting wave front is evident from the high-speed video recordings. Further, the missing wall friction and turbulence modelling may lead to inaccuracies in the overtopping volume from the jet. These stages of the flow, however, are characterized by significant mixing of water and air, spray generation and break-up of bubbles that makes a detailed numerical description difficult. In this perspective, the present approach can be considered as a first simplistic attempt to model the main flow of the impact and overtopping.

The main factor for a good numerical reproduction of impact and overtopping flow is an accurate reproduction of the incident

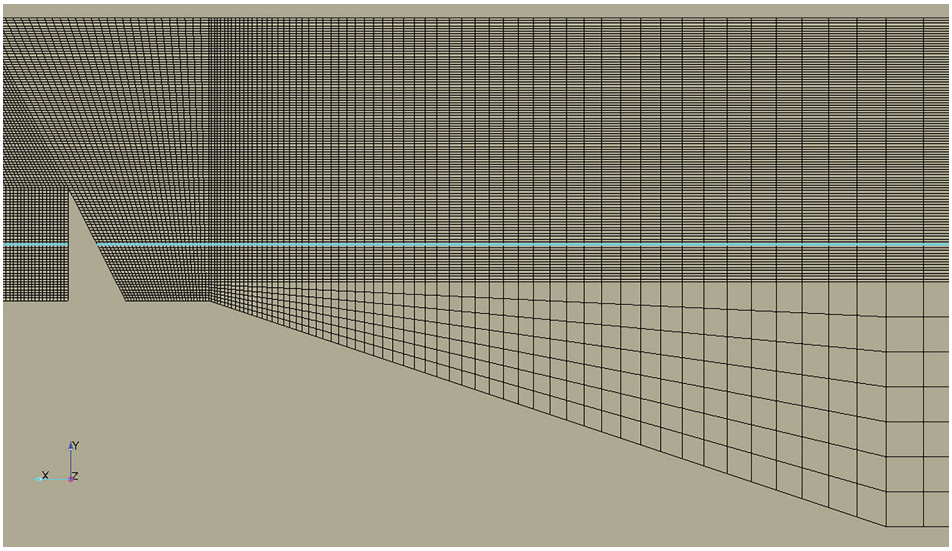

Figure 3 The numerical grid in the berm and wall region. The thick horizontal line is the still water level

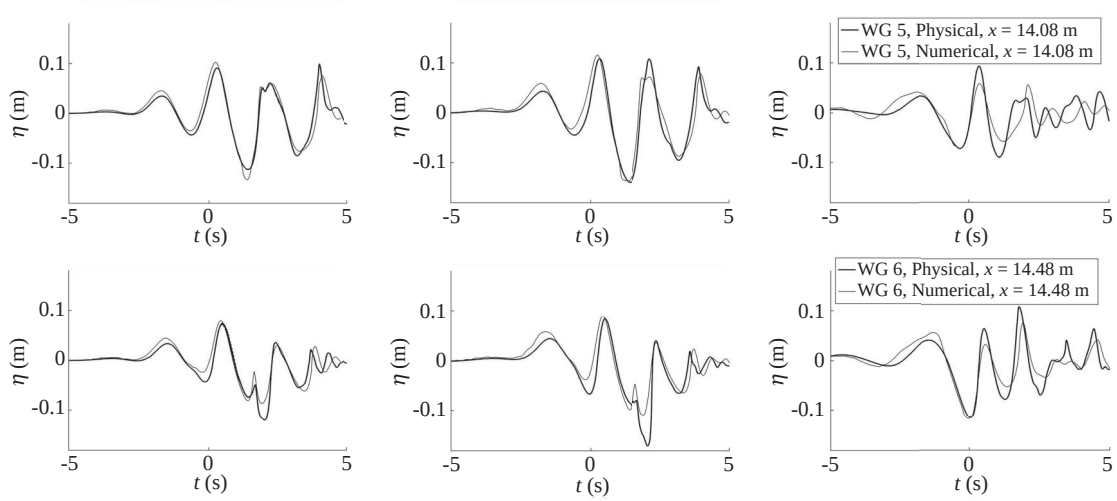

Figure 4 Predicted and measured free surface elevation time histories: left-hand column – group producing steep-fronted breaker; middle column – group producing plunging breaker; right-hand column – group producing broken wave

wave profile prior to impact. In the experiment, the wave paddle was moved according to linear theory and a system of bound and free second-order waves is created (e.g. Schäffer & Steenberg, 2003). Analysis of the second-order long waves associated with the propagation of focused wave groups can be found in Orszaghova, Taylor, Borthwick, and Raby (2014), Fitzgerald et al. (2016) and Whittaker et al. (2017). The long waves travel faster than the main waves of the group and lead to an apparent varying mean water level in the flume. This is especially important at the wall, where the shape of the impacting wave is strongly sensitive to the local depth (e.g. Peregrine et al., 2004).

To reproduce the experimental waves, wave generation was based on linear analysis of the measured free surface elevation of the first four wave gauges in the deep-water region of the flume (Bredmose et al., 2010). The extracted linear description of the incident wave field was next applied in the Navier–Stokes solver in a relaxation zone at $x = [-5\ 0]$ m, where $x = 0$ corresponds to the wave maker position. While this approach does not constitute direct modelling of the moving wave maker, it resembles the forcing of linear wave motion at the wave maker position and thus allows for a partial reproduction of the second-order effects.

Time histories of the numerical and measured free surface elevations are shown in Fig. 4 for wave gauges 5 and 6. In the left column is the group that produces the steep-fronted breaking wave. The good match for the group shape and for the individual waves at WG5 is representative for the other wave gauges in the flume. Some deviations are seen at WG6. This may be explained by the enhancement of nonlinearity at the reduced depth and the reduction of temporal separation between the incident and reflected waves in this region. The wave causing the

overtopping is the one that passes WG5 just after $t = 0$ s. The crest height of this wave is well reproduced at WG6, although there is a tendency for the numerical results to over-predict the mean water level for this part of the signal. Such apparent variations of the mean water level may be due to the presence of bound and spurious long waves in the flume as discussed above. The results for the wave group that produces the plunging wave event (middle column) are very similar to those of the steep-fronted wave.

The right column shows results for the group that produces the already-broken wave, which was generated with a top-hat spectrum rather than a JONSWAP spectrum. For this spectrum, the focusing process is more pronounced with an initial strong content of short waves at WG1 (not shown here), followed by longer and taller waves that travel faster. The under-prediction of the crest height for the main overtopping wave at WG5 and 6 may be linked to insufficient reproduction of the shortest waves in the model. A good match for the trough depth, however, is achieved at WG6.

5 Overtopping observations and results

5.1 *Wave overtopping behaviour*

The overtopping characteristics of the physical and numerical models are compared in Fig. 5a–c for the steep-fronted, plunging and broken waves respectively, for the lowest wall crest elevation of 150 mm above SWL. The video frames shown are for times (t') relative to wave impact in the physical experiments. The computer-generated images were synchronized to the initial stages of wave–structure interaction by eye.

Steep-fronted wave overtopping

At $t' = -0.05$ s in Fig. 5a, the front of the wave is almost vertical and the flow converges towards an impact zone. The impact at $t' = 0.00$ s traps a small pocket of air which is also captured in the numerical solution. Both the physical and numerical records show ($t' = 0.05$ s) that an upward jet is formed after the impact, but the numerical solution is too coarse to capture the details of spray formation and break-up of the air pocket into small bubbles. As the numerical model does not include surface tension, a detailed description of these flow features is unlikely to be obtained even with a very fine grid.

The numerical model provides a satisfactory representation of the overall flow which initiates overtopping just prior to $t' = 0.10$ s. Trapped air is present along the wall until $t' = 0.20$ s where, numerically and experimentally, the underside of the overtopping tongue of water is no longer tangential to the wall. This illustrates the free fall of the water under gravity and may define the beginning of an intermediate region between the jet-like and quasi-steady overflow. At $t' = 0.35$ s the physical overtopping reaches the collection tank. Consequently, spatial comparisons are invalid beyond the tank, whereas, up to it, the overall shapes of the flows are still in close agreement. By $t' = 0.40$ s, both models indicate that the upward velocity of the flow over the wall has become so small that its initial trajectory is effectively horizontal before it falls under gravity. The horizontal velocity decreases as the depth of flow over the crest decreases as seen at $t' = 0.50$ s. Splashing is captured in the last frame, and overtopping ceases just after $t' = 0.60$ s.

Plunging wave overtopping

Comparisons of the plunging wave overtopping event are provided in Fig. 5b. The frames for $t' = (-0.05\text{ s},\ 0.00\text{ s})$ show the wave just before and at the time of impact. While an air pocket is trapped in both cases, and the experimental and numerical impact shapes are similar, the physical wave traps significantly more air than the numerical wave. As for the steep-fronted event, spray and bubble break-up occur physically at $t' = 0.05$ s, but are beyond the grid scale of the numerical solution. At $t' = 0.10$ s, the physical flow exhibits overtopping spray. In the numerical solution this is represented by a small droplet ejected from the main flow in the direction tangential to the wall. For the frames from $t' = 0.15$ s to $t' = 0.25$ s, the shapes of the overtopping flows agree well but bubbles persist along the wall in the physical model when the numerical model shows no evidence of entrained air. From $t' = 0.25$ s onwards the flow appears to resemble a quasi-steady weir-like flow with air trapped under the nappe. This is illustrated by the persistent footprint of the initial air pocket as a "notch" in the underside of the overtopping tongue.

The physical overtopping hits the back screen of the overtopping tank just before $t' = 0.35$ s, limiting spatial comparisons as before. Otherwise, the flow profiles in the two models are in very good agreement throughout the event.

Broken wave overtopping

As shown in Fig. 5c, the physical and numerical results for the broken-wave overtopping were in less agreement than they were for the plunging and steep-fronted wave cases. This can be attributed to the under-prediction of the overtopping wave height at WG6 in the numerical model, see Fig. 4. At $t' = -0.05$ s, the numerical wave has overturned, with part of it touching down onto the free surface of the water at the offshore edge of the berm, while at the same time the physical wave is about to touch down close to the toe of the wall. In both events, a new jet emerges landward of the initial touch-down, with subsequent uprush along the wall. The video reveals the three-dimensional nature of the broken wave, with undulations in the wave surface across the channel due to transverse instability arising from the breaking process. At $t' = 0.00$ s, the two events show large trapped air pockets, wall impact, and uprush. Although the numerical uprush starts much earlier than its physical counterpart the flows remain similar in the following frames. At $t' = 0.15$ s, a large volume of water separates from the main overtopping tongue in the numerical solution. This is consistent with the large

Figure 5 Comparison of numerical model output and video frame sequence for (a) steep-fronted wave; (b) plunging wave; and (c) broken wave overtopping of 150 mm freeboard wall

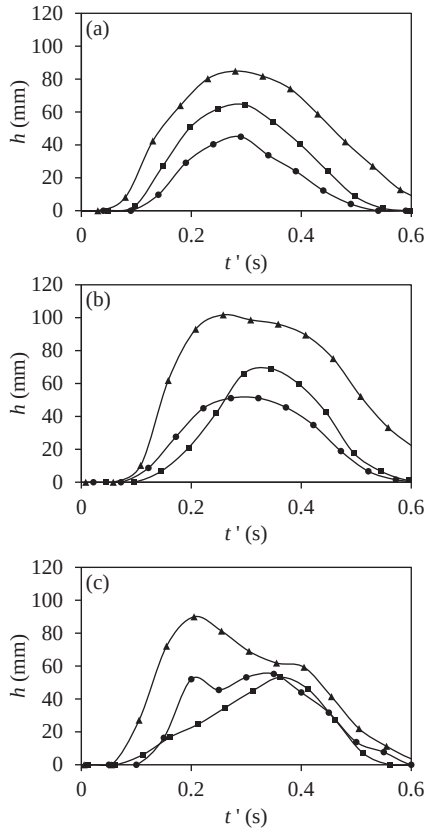

Figure 6 Overtopping flow layer thickness at seaward edge of the wall for (a) steep-fronted wave; (b) plunging wave; and (c) broken wave. ▲: 150 mm freeboard, ■: 200 mm freeboard, ●: 250 mm freeboard

velocities and spray/droplet expulsion observed in the physical flow.

Entrained air continues to be present in the flow up the offshore side of the wall for the remainder of the event, although the numerical air pockets do not break up into small bubbles as they do in the physical model. Despite the discrepancy in the initial impact shape, the general free surface shape is quite similar after $t' = 0.15$ s. This in turn leads to the overtopping flow having a similar shape in both models.

Further details of the water particle kinematics obtained both from the numerical model and the BIV technique are presented in Supplemental Material S2.

5.2 *Overtopping flow depth*

The variation of the vertical depth of flow (h) over the wall's crest gives further insight into the overtopping process (Van Gent, 2002). Values of h estimated from calibrated video frames of the physical model are plotted against t' for the three crest elevations in Fig. 6. Some of the estimates were a little subjective, particularly for the broken wave which entrained numerous bubbles. The 3D nature of the surface across the channel also led to some uncertainty regarding the precise depth of flow in the centre of the channel where the overtopping falls into the collection box.

Figure 6 shows that lower freeboards lead to longer and deeper overtopping, and that the events for the steep and plunging waves with the highest freeboard exhibit a degree of temporal symmetry. Other events are much less symmetrical with either a relatively fast initial rate of change (e.g. the plunging and broken waves with 150 mm freeboard) or a relatively slow one (e.g. the plunging and broken waves with 200 mm freeboard). There are no consistent trends within the plunging and broken wave events as, in both cases, the overtopping flow with 250 mm freeboard again has a relatively fast initial rate of change of flow depth. Figure 5 shows these breaker types entrain substantial quantities of air; this two-phase flow may well cause the depth-time histories to be irregular. The plunging wave tests with 150 mm freeboard exhibit rapid increases in depth up to the maximum value before a gentler decrease down towards zero. The rapid increase corresponds to high velocities associated with the jet (also see Fig. S2-2). Finally, given that the bulk of the overtopping flow occurs after $t' = 0.2$ s for all three wave types, the quasi-steady overflow clearly provides the most significant contribution to the overtopping volume.

5.3 *Overtopping volume – measurement and estimation*

Direct measurement of the overtopping volumes using the physical model is considered below. Then methods for estimating the volumes by use of BIV, the numerical model, and a simple weir analogy are outlined. Finally, results obtained by all four methods are compared.

Direct measurement

Overtopping measurements were taken for all three breaker types and wall-crest elevations. Because the smallest and most variable volumes were collected with a 250 mm freeboard, 10 repeat tests were undertaken. For the other two freeboards only three or four repeats were obtained. Table 2 presents mean (M), minimum and maximum overtopping results for all tests, and standard deviations where 10 repeats were used.

Comparison with Table 1 again illustrates the limitations of using simple wave height values, as the plunging wave generates more overtopping than the broken wave, despite appearing to have a lower height at the toe of the berm. The variability of the measured volumes is greatest for broken waves and least for steep-fronted waves. It is not surprising that identical breaking waves produce a range of overtopping volumes as the breaking process is highly turbulent. In investigations of this nature it is not unusual to repeat the experiments several times to achieve an average result. Ryu and Chang (2008) repeated their overtopping tests 10 times and seem to have a standard deviation of a little under 5% in the volumes obtained for plunging breakers on a deep-water laboratory structure. Kortenhaus et al. (2004) suggest that overtopping rates may vary by up to 12% in repeat tests, hence results presented here are fairly typical. Furthermore, it must be borne in mind that the overtopping caused by a wave is affected by other waves in the sequence. In random

Table 2 Mean (M), minimum and maximum measured overtopping volumes

	Steep-fronted wave				Plunging wave				Broken wave			
Freeboard (mm)	mean, M (l m^{-1})	min	max	% standard deviation	mean, M (l m^{-1})	min	max	% standard deviation	mean, M (l m^{-1})	min	max	% standard deviation
150	14.29	1.00 M	1.00 M	N/A	19.31	1.00 M	1.01 M	N/A	14.03	0.94 M	1.05 M	N/A
200	8.19	0.97 M	1.05 M	N/A	11.64	0.99 M	1.01 M	N/A	9.89	0.98 M	1.04 M	N/A
250	4.00	0.92 M	1.06 M	4%	8.08	0.92 M	1.08 M	5%	6.48	0.7 M	1.21 M	14%

waves, McCabe et al. (2013) found that overtopping varied by as much as 25%.

Estimation techniques – BIV

Overtopping volumes were estimated from flow rates based on the temporal variation of the BIV velocity vectors and depths at the crest of the wall. Only the steep-fronted wave tests were considered because of the difficulty of estimating vertical depths in the highly-aerated flows produced by the other breaker types. Ryu and Chang (2008) also question the accuracy of flow rates in highly-aerated water when no measure of void fraction is available.

Estimation techniques – numerical model

The numerical model estimated volumes by time integration of the flow discharge over the wall's crest. All three wave types were considered, but for the lowest wall freeboard only.

Estimation techniques – weir analogy

This approach assumes that the flow over the wall is pseudo-steady and that, at each instant of time, it is analogous to flow over a vertical-plate sharp-crested weir with a detached nappe. The overtopping discharge at any instant can then be estimated by use of the standard discharge relationship (Hamill, 2001):

$$q_t = 2/3 C_d (2g)^{1/2} H^{3/2} \tag{2}$$

where q_t is the theoretical discharge per unit length, C_d is the discharge coefficient given by:

$$C_d = 0.602 + 0.083\, H/P \tag{3}$$

and where H is the upstream head, P is the height of the weir and g is the acceleration due to gravity. In order to apply these relationships to the model coastal structure, H is equated to the depth of flow over the wall's crest and P to the wall's height as shown in Fig. 7. It is conceded that the analogy suffers from the fact that overtopping flow is unsteady and that H is measured at the crest rather than upstream. In the case of a weir, measuring H at its crest would reduce the magnitude of H and hence the discharge predicted by Eq. (2). Whereas, inclining the weir plate to match the slope of the wall would be expected to increase the value of C_d and hence increase the predicted discharge. Thus, the errors in these approximations may to some extent counteract each other. From the estimated instantaneous discharges it is possible to estimate the overtopped volume by numerically integrating over time.

Comparisons

Results from the three estimation methods are shown alongside the measured volumes in Fig. 8 as follows:

- Figure 8a shows that, for the steep-fronted wave, both the BIV and numerical model estimates are within 7% of the measured volumes. For BIV this is comparable to the accuracy of the estimated velocities at the crest of the wall (Fig. S1-2e) while the single numerical result is a relatively small over-estimate. The weir analogy tends to under-predict with the estimate for the smallest volume being within 0.3% and all the estimates within 20%.
- Figure 8b shows the results for the plunging wave. This time the numerical model over-predicts by 12%. The weir analogy

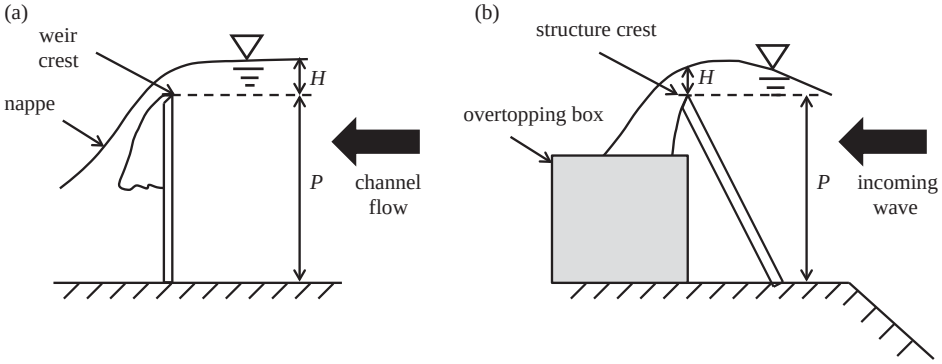

Figure 7 Schematic diagram of fluid-structure problems: (a) channel flow over a flat plate weir; and (b) overtopping flow over a simple laboratory coastal structure

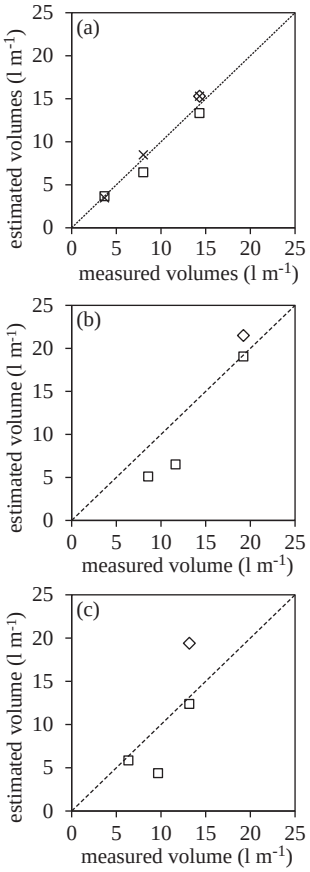

Figure 8 Estimated overtopping volumes compared with measured overtopping volumes for (a) steep-fronted wave; (b) plunging wave; and (c) already broken wave: ×, BIV; ◊, numerical model; □, weir analogy

predicts one of the three volumes to within 1% but the other two are under-predicted by about 40%.

- Finally, relative to the overtopping volumes measured for the already-broken wave, Fig. 8c shows that the numerical model over-predicts by 47%; and the weir analogy is surprisingly good for two volumes but under-predicting by 55% for one.

6 Discussion and conclusions

The characteristics of the overtopping caused by a steep-fronted, a plunging and a broken wave over a 27° sloping wall of variable height were investigated by means of a physical model of sufficient size to be predictive for a geometrically similar full-scale situation by application of the Froude law. Here, no scaling of the overtopping has been carried out. Instead, the measured volumes have been compared with estimates obtained by use of BIV, a numerical model, and a weir analogy. However, when considering the results, it should be remembered that physical models are susceptible to scale effects. Thus, relative to a full-scale situation, over-sized viscous and surface tension forces will have respectively reduced the overtopping and increased the size of both bubbles and spray droplets.

Each type of breaker in the physical model was produced by use of a focused wave group and the incident wave shown to be highly repeatable. However, the measured overtopping was significantly more variable. The degree of variability tended to increase with the level of aeration and turbulence which also caused the flow to be less two-dimensional. Thus, for a particular wall height, the repeatability tended to be greatest when the steep-fronted wave was used and least when the broken wave was used. The flow depths commonly used to characterize wave overtopping were shown (Fig. 6) to exhibit greater temporal symmetry for the steep-fronted wave than for the other more highly aerated waves. The fact that there was not a consistent initial rapid increase in flow contrasts with findings on more gentle slopes (Hunt-Raby et al., 2011; Schüttrumpf & Oumeraci, 2005). There was also evidence that jets caused a more rapid increase in the depth of the overtopping flow at the lowest freeboard than they did at the higher freeboards. This may imply that overtopping jets could be more hazardous than expected during high tides. However, the jets contributed only a small proportion of the overtopping volume despite their relatively high velocities.

BIV was used to estimate flow velocities. The level of aeration and turbulence associated with the plunging and broken waves made it difficult to estimate the depth of flow at the crest of the wall from video recordings. Consequently, the temporal variation in the velocity and depth at the crest were only used to estimate the overtopping for tests using the steep-fronted wave. The results were found to be within 7% of the measured values. This suggests that, in favourable circumstances, BIV could be a viable alternative to direct measurement, particularly as further improvement in the technique may be possible by averaging velocities over a larger number of repeats. This was done by Rivillas-Ospina et al. (2012) who repeated their BIV experiments 20 times when investigating plunging wave impacts on beaches.

The numerical model was based on a two-phase incompressible Navier–Stokes solver that enabled trapped air pockets to be reproduced, although the subsequent break up into small bubbles was beyond the grid resolution used. The model was generally found able to reproduce well both the variation in water surface elevation of the incident waves and the subsequent overtopping flow, although the details of spray generation were not captured. Like high-speed camera footage of the physical model, the numerical model indicated that there were two fairly distinct phases in the overtopping process for all three of the wave types investigated, i.e. first a jet which lasted for around 0.2 s followed by quasi-steady flow. The behaviour of the steep-fronted and plunging events was very similar, although the plunging wave trapped more air. However, the broken wave showed quite different characteristics for the jet formation, with considerably more trapped air. For this event, there was a large difference between the physical and numerical wave profiles at the time of impact (Section 4.3) and the physical flow was less two-dimensional across the channel.

The numerical model produced satisfactory agreement of overtopping with measured values, particularly for the steep-fronted and plunging breaker, while larger over-prediction was seen for the already-broken wave due to pronounced differences in the wave shape prior to wall impact, the increased mixing and turbulence of the flow after impact and to some extent the lack of wall friction. Modelling the turbulence would be a severe test for any numerical model. The fact that the discrepancy was never greater than 12% for the steep-fronted and plunging waves suggests that a numerical model can be used to predict overtopping despite the occurrence of significant wave impacts, without the expense of constructing and running physical models.

The simplistic use of steady flow relationships in the weir analogy consistently under-predicted the measured volumes by between 0.3 and 55%, the smallest difference occurring with the steep-fronted waves and the largest with the broken waves. Whilst the tendency to under-predict could be eliminated by increasing the value of C_d, the necessary magnitude of the increase may always depend on both the wave conditions and the structural geometry, as it would for the situations considered in this paper. With appropriate calibration studies the weir analogy has the potential to become a reliable means of estimating the overtopping caused by individual waves.

Focused wave groups have recently been demonstrated to reliably reproduce conditions close to the worst-case situations found in a random sea-state in the coastal zone (Whittaker, Raby, Fitzgerald, & Taylor, 2016). The investigation presented in this paper hence provides an efficient method to model genuine extreme wave interactions with coastal structures, revealing the sensitivity of wave overtopping behaviour to specific breaking wave types. A better understanding of these individual wave events is crucial to the safety of people and infrastructure at the coast.

Acknowledgements

Bo Terp Paulsen, DTU, is thanked for extensive help on setting up the OpenFOAM computations, as are Thulasikopan Kirubakaramoorthy, Masud Alom and Haileab Takeste MSc students at the University of East London who undertook some elements of the BIV analysis. Finally, the authors wish to acknowledge the debts owed to Howell Peregrine, the project PI at Bristol who passed away shortly after the project started, and to Andrew Hogg who subsequently took administrative responsibility for Bristol's contribution.

Funding

The OVI project (Fundamentals of Overtopping from individual Violent water wave Impacts) was supported by the Engineering and Physical Sciences Research Council (EP/D080754/1 and EP/D080533/1).

Supplemental data

Supplemental material for this article can be accessed doi:10.1080/00221686.2018.1555549.

Notation

C_d	=	discharge coefficient of a weir (–)
D	=	internal depth of overtopping box (m)
g	=	acceleration due to gravity (m s^{-2})
h	=	overtopping depth (mm)
H	=	upstream head above the crest of a weir (m)
H_{m0}	=	significant wave height (m)
k_n	=	wave number (m^{-1})
L	=	internal length of overtopping box (m)
$L_{\mathrm{m}-1,0}$	=	deep water wavelength (m)
M	=	mean measured overtopping volume (l m^{-1})
n	=	counter for the sum of the individual Fourier components combined to create a wave group (-)
P	=	height of a weir (m)
q_{t}	=	theoretical discharge per unit length of a weir (m^3 s^{-1})
S_η	=	wave spectrum (m^2 s)
t	=	time (s)
t_0	=	focus time (s)
t'	=	time, with respect to time of impact (s)
W	=	internal width of overtopping box (m)
x	=	position, with respect to the paddle (m)
x_0	=	focus location, with respect to the paddle (m)
α	=	crest height (m)
β	=	structure slope
η	=	surface elevation (m)
$\xi_{m-1,0}$	=	Iribarren number
σ	=	standard deviation of the free surface elevation (m)
ω_n	=	frequency (Hz)
$\Delta\omega$	=	frequency discretization (Hz)

References

Antoine, A. L. C. (2009). *Dynamics of wave breaking at a coastal sea wall* (MSc dissertation). Texas A&M University.

Baldock, T. E., Swan, C., & Taylor, P. H. (1996). A laboratory study of nonlinear surface waves on water. *Philosophical Transactions of the Royal Society of London. Series A: Mathematical, Physical and Engineering Sciences*, *354*, 649–676.

Besley, P. (1999). *Overtopping of seawalls – Design and assessment manual*. R & D Technical Report W 178, ISBN 1 85705 069 X. Bristol, UK: Environment Agency.

Bredmose, H., Hunt-Raby, A., Jayaratne, R., & Bullock, G. N. (2010). The ideal flip-through impact: Experimental and numerical investigation. *Journal of Engineering Mathematics*, *67*(1–2), 115–136.

Bruce, T., van der Meer, J., Pullen, T., & Allsop, W. (2010). Wave overtopping at vertical and steep structures. Chapter 16 in Y. C. Kim (Ed.), *Handbook of coastal and ocean engineering* (pp. 411–439). Singapore. Hackensack, NJ: World Scientific.

Bullock, G. N., & Murton, G. J. (1989). Performance of a wedge-type absorbing wave maker. *Journal of Waterway, Port, Coastal, and Ocean Engineering*, *115*(1), 1–17.

Burcharth, H. F., & Hughes, S. A. (2006). Fundamentals of design. *Coastal engineering manual 4, Chapter VI-5–2 Design of coastal project elements*, S. A. Hughes, ed. Engineer Manual 1110-2-1100. U.S. Army Corps of Engineers, Washington, DC.

De Rouck, J., & Van de Walle, B. (2001). Exploitation and dissemination of results. *OPTICREST Research Report on Task 6*.

De Rouck, J., Verhaeghe, H., & Geeraerts, J. (2009). Crest level assessment of coastal structures – General overview. *Coastal Engineering*, *56*(2), 99–107.

Dean, R. G., Rosati, J. D., Walton, T. L., & Edge, B. L. (2010). Erosional equivalences of levees: Steady and intermittent wave overtopping. *Ocean Engineering*, *37*, 104–113.

Deshpande, S. S., Anumolu, L., & Trujillo, M. F. (2012). Evaluating the performance of the two-phase flow solver interFoam. *Computational Science & Discovery*, *5*, 014016.

Dold, J. W., & Peregrine, D. H. (1986). An efficient boundary-integral method for steep unsteady water waves. In K. W. Morton & M. J. Baines (Eds.), *Numerical methods for fluid dynamics II* (pp. 671–679). Oxford: Oxford University Press.

EurOtop. (2016). Manual on wave overtopping of sea defences and related structures. An overtopping manual largely based on European research, but for worldwide application. Van der Meer, J.W., Allsop, N.W.H., Bruce, T., De Rouck, J., Kortenhaus, A., Pullen, T., Schüttrumpf, H., Troch, P. & Zanuttigh, B.

Fitzgerald, C. J., Taylor, P. H., Orszaghova, J., Borthwick, A. G. L., Whittaker, C., & Raby, A. C. (2016). Irregular wave runup statistics on plane beaches: Application of a Boussinesq-type model incorporating a generating–absorbing sponge layer and second-order wave generation. *Coastal Engineering*, *114*, 309–324.

Hamill, L. (2001). *Understanding hydraulics* (2nd ed.). Basingstoke: Palgrave.

Hughes, S. A., & Nadal, N. C. (2009). Laboratory study of combined wave overtopping and storm surge overflow of a levee. *Coastal Engineering*, *56*, 244–259.

Hughes, S. A., & Thornton, C. I. (2016). Estimation of time-varying discharge and cumulative volume in individual overtopping waves. *Coastal Engineering*, *117*, 191–204.

Hunt-Raby, A., Borthwick, A. G. L., Stansby, P. K., & Taylor, P. H. (2011). Experimental measurement of focused wave group and solitary wave overtopping. *Journal of Hydraulic Research*, *49*(4), 450–464.

Jacobsen, N. G., Fuhrman, D. R., & Fredsøe, J. (2011). A wave generation toolbox for the open-source CFD library: OpenFoam. *International Journal of Numerical Methods in Fluids*, *70*, 1073–1088. doi:10.1002/fld.2726

Jayaratne, R., Hunt-Raby, A., Bullock, G., & Bredmose, H. (2008). Individual violent overtopping events: New insights. *31st International Conference on Coastal Engineering*, pp. 2983–2995.

Kortenhaus, A., Oumeraci, H., Geeraerts, J., De Rouck, J., Medina, J. R., & Gonzalez-Escriva, J. A. (2004). *Laboratory effects and other uncertainties in wave overtopping measurements*. Proc. 29th Int. Conf. Coastal Engineering, Lisbon, Portugal.

Kway, J. H. L., Loh, Y., & Chan, E. (1998). Laboratory study of deep-water breaking waves. *Ocean Engineering*, *25*(8), 657–676.

Madsen, P. A., & Sørensen, O. R. (1992). A new form of the Boussinesq equations with improved linear dispersion characteristics. Part 2. A slowly-varying bathymetry. *Coastal Engineering*, *18*, 183–204.

McCabe, M. V., Stansby, P. K., & Apsley, D. D. (2013). Random wave runup and overtopping a steep sea wall: Shallow-water and Boussinesq modelling with generalised breaking and wall impact algorithms validated against laboratory and field measurements. *Coastal Engineering*, *74*, 33–49.

Nørgaard, J. Q. H., Andersen, T. K., Burcharth, H. F., & Steendam, G. J. (2013). Analysis of overtopping flow on sea dikes in oblique and short-crested waves. *Coastal Engineering*, *76*, 43–54.

Orszaghova, J., Borthwick, A. G. L., & Taylor, P. H. (2012). From the paddle to the beach – A Boussinesq shallow water numerical wave tank based on Madsen and Sørensen's equations. *Journal of Computational Physics*, *231*, 328–344.

Orszaghova, J., Taylor, P. H., Borthwick, A. G. L., & Raby, A. C. (2014). Importance of second-order wave generation for focused wave group run-up and overtopping. *Coastal Engineering*, *94*, 63–79.

Paulsen, B. T., Bredmose, H., & Bingham, H. B. (2014). An efficient domain decomposition strategy for wave loads on surface piercing circular cylinders. *Coastal Engineering*, *86*, 57–76.

Pearson, J., Bruce, T., & Allsop, N. W. H. (2002). *Violent wave overtopping – Measurements at large and small scale*. 28th International Conference on Coastal Engineering, Cardiff, pp. 2227–2238.

Peregrine, D. H., Bredmose, H., Bullock, G. N., Obhrai, C., Müller, G., & Wolters, G. (2004). *Water wave impact on walls and the role of air*. 29th International Conference on Coastal Engineering, Lisbon, pp. 4005–4017.

Rivillas-Ospina, G., Pedrozo-Acuna, A., Silva, R., Torres-Freyermuth, A., & Gutierrez, C. (2012). Estimation of the velocity field induced by plunging breakers in the surf and swash zones. *Experiments in Fluids*, *52*, 53–68.

Ryu, Y., & Chang, K. A. (2008). Green water void fraction due to breaking wave impinging and overtopping. *Experiments in Fluids*, *45*, 883–898.

Ryu, Y., Chang, K. A., & Lim, H. J. (2005). Use of bubble image velocimetry for measurement of plunging wave impinging on structure and associated green water. *Journal of Measurement Science and Technology*, *16*, 1945–1953.

Ryu, Y., Chang, K. A., & Mercier, R. (2007). Runup and green water velocities due to breaking wave impinging and overtopping. *Experiments in Fluids*, *43*, 555–567.

Schäffer, H. A., & Steenberg, C. M. (2003). Second-order wavemaker theory for multidirectional waves. *Ocean Engineering*, *30*, 1203–1231.

Schüttrumpf, H., & Oumeraci, H. (2005). Layer thicknesses and velocities of wave overtopping flow at seadikes. *Coastal Engineering*, *52*, 473–495.

Stansby, P. K., Xu, R., Rogers, B. D., Hunt, A. C., Borthwick, A. G. L., & Taylor, P. H. (2008). *Modelling tsunami overtopping of a sea defence by shallow-water Boussinesq, VOF and SPH methods*. Oxford, UK: Floodrisk2008, 255–261.

Van der Meer, J. W., & Janssen, J. P. F. M. (1995). Wave run-up and wave overtopping at dikes. In N. Kobayashi & Z. Demirbilek (Eds.), *Wave forces on inclined and vertical wall structures* (pp. 1–27). New York, NY: ASCE.

Van Gent, M. (2002). Measurement of velocities and the thickness of water-layers on the crest and inner slope of dikes. *Delft Cluster Low-exceedence wave overtopping events DC030202/H3803*. Delft Hydraulics.

Watanabe, Y., & Ingram, D. M. (2016). Size distributions of sprays produced by violent wave impacts on vertical sea walls. *Proceedings of the Royal Society A: Mathematical, Physical and Engineering Science*, *472*, 20160 423.

Whittaker, C. N., Fitzgerald, C. J., Raby, A. C., Taylor, P. H., Orszaghova, J., & Borthwick, A. G. L. (2017). Optimisation of focused wave group runup on a plane beach. *Coastal Engineering*, *121*, 44–55.

Whittaker, C. N., Raby, A. C., Fitzgerald, C. J., & Taylor, P. H. (2016). The average shape of large waves in the coastal zone. *Coastal Engineering*, *114*, 253–264.